Determining Bishop's parameter χ based on pore size distribution

Geng Niu, Yu-Jun Cui, Jean-Michel Pereira, Longtan Shao, De'an Sun

Determining Bishop's parameter χ based on pore size distribution

Geng Niu[1], Yu-jun Cui[2], Jean-Michel Pereira[2], Longtan Shao[1], De'an Sun[3]

[1]Department of Engineering Mechanics, Dalian University of Technology, 116024 Dalian, Liaoning, China
[2]Navier, Ecole des Ponts, Univ Gustave Eiffel, CNRS, Marne-la-Vallée, France
[3]Department of Civil Engineering, Shanghai University, 200444 Shanghai, China

[*]**Corresponding author:**

Prof. Yu-Jun CUI
Ecole des Ponts ParisTech
6-8 av. Blaise Pascal, Cité Descartes, Champs-sur-Marne
F-77455 Marne-la-Vallée cedex France
Telephone: +33 1 64 15 35 50
Fax: +33 1 64 15 35 62
E-mail: yujun.cui@enpc.fr

Abstract

Extension of the effective stress concept to unsaturated soils has been a major concern for decades. Recent studies significantly contributed to the understanding of the fundamentals behind Bishop's parameter χ which is generally used to define the effective stress for unsaturated soils. Examination of the recently proposed methods showed that the contribution of suction to effective stress was often overestimated, especially in high suction range. In this study, considering that soil pores with different sizes contribute differently to the overall hydro-mechanical behaviour, a new method to determine Bishop's parameter χ is proposed. The key variable used in this method is the ratio of the change in water volume to the change in macro-pore void volume due to loading at constant suction. Shear strength data for a weakly expansive clay were used for validation. A good agreement was obtained between prediction and measurement, indicating the validity of the proposed method.

Keywords:

constitutive relations; fabric/structure of soils; shear strength; partial saturation; suction

NOTATION

e_{w2}	water ratio caused by change of strain at constant suction
e_w^m	microscopic water ratio
e^m	microscopic void ratio
S_r^e	effective degree of saturation
S_r^m	microscopic degree of saturation
S_r^{cap}	capillary degree of saturation
S_r^{ads}	adsorbed degree of saturation
s_m	suction corresponding to the median pore diameter
V_{w1}	water volume governed by suction
α	ratio of the change in incremental water volume caused by the change of strain under constant suction to total pore volume increment
λ	material parameter defining the effective degree of saturation
ξ	standard deviation of the log-transformed pore radius
φ	fitting parameter related to the theoretical degree of saturation due to adsorption at 1 kPa suction
χ	Bishop's effective stress parameter

INTRODUCTION

The definition of stress variables is essential in developing constitutive models for unsaturated soils. There are two approaches for modeling their mechanical behaviour: the effective stress approach (Bishop, 1959) and the two independent state variables approach (Coleman 1962, Fredlund & Morgenstern, 1977). Currently, using two independent stress variables to describe the behavior of unsaturated soils is widely accepted (Cui and Delage, 1996; Wheeler *et al*., 2003; Liu *et al*., 2018). Bishop stress is often considered as one variable in the two independent stresses approach, because it represents a smooth extension of Terzaghi's effective stress (Sheng *et al*., 2004; Pereira *et al*., 2005; Zhou *et al*., 2018). In the Bishop's effective stress concept, the key parameter is χ, as shown in Eq. 1 (Bishop, 1959):

$$\sigma' = \sigma - [\chi u_{\mathrm{w}} + (1-\chi)u_{\mathrm{a}}] \tag{1}$$

where σ' is unsaturated effective stress; σ is total stress; χ is the effective stress parameter (Bishop's parameter); u_{w} and u_{a} are water and air pressures, respectively.

In the past few decades, various criteria were reported for determining χ. In the early contributions (Bishop & Blight, 1963), χ was set equal to degree of saturation S_{r}:

$$\chi = S_{\mathrm{r}} \tag{2}$$

which is the simplest, and most used assumption to date. But several studies showed that this choice significantly overestimates the contribution of suction to effective stress, especially in the high suction range (Sheng *et al*., 2011; Zhou *et al*., 2016). In a later effort, the overestimation was reduced by using an effective degree of saturation (Vanapalli *et al*., 1996). To define this latter, attempts have been made to

directly relate χ to the total degree of saturation, such as (Vanapalli *et al*., 1996):

$$\chi = f(S_{\mathrm{r}}) = (S_{\mathrm{r}})^{\lambda} \tag{3}$$

where $\lambda \geq 1$ is a material parameter. For coarse-grained soils, parameter λ is almost equal to unity, while for fine-grained soils λ is larger than unity. Garven & Vanapalli (2006) found that λ is correlated with plasticity index, I_{p}.

Soil water consists in capillary water and adsorbed one. Since adsorbed water is strongly bonded to soil particles (Lu *et al*., 2010; Konrad & Lebeau, 2015; Zhou *et al*., 2016; Gao *et al*., 2018), it does not contribute to the contact stress and thus to the effective stress. Thereby, Zhou *et al*. (2016) related the Bishop's parameter χ to the capillary degree of saturation $S_{\mathrm{r}}^{\mathrm{cap}}$ which is the difference between the total degree of saturation and the adsorbed degree of saturation $S_{\mathrm{r}}^{\mathrm{ads}}$:

$$\chi = S_{\mathrm{r}}^{\mathrm{cap}} = \frac{\mathrm{C}(s) - \varphi \mathrm{C}(s)\mathrm{A}(s)}{1 - \varphi \mathrm{C}(s)\mathrm{A}(s)} \tag{4}$$

$$\text{with } C(\mathrm{s}) = \frac{1}{2}\mathrm{erfc}\left[\frac{\ln(s/s_{\mathrm{m}})}{\sqrt{2}\xi}\right],\ A(\mathrm{s}) = 1 - \frac{\ln(s)}{\ln(s_{\mathrm{d}})}$$

where s is matric suction; φ and ξ are fitting parameters determined by soil water retention curve (SWRC); s_{m} is the suction which corresponds to the median pore diameter; s_{d} is the suction at extreme dry state, assumed equal to 10^6 kPa. However, the lastest investigation showed that using capillary degree of saturation underestimates the contribution of suction to Bishop's effective stress for most soils (Gao *et al*., 2020). It has been well documented that for compacted soils, the microstructure is characterised by two pore populations: i) macro-pores where capillary effects dominate, and ii) micro-pores where the hygroscopic effect dominates (Romero & Vaunat, 2000; Alonso *et al*., 2010). It has been admitted that

107 the contribution of suction to Bishop's effective stress is only related to the water
108 trapped in macro- or inter-aggregate pores (Alonso *et al*., 2010; Zhai *et al*., 2019).
109 This was confirmed by some experimental results which showed that loading and
110 drying paths predominantly influenced the macropores, while micropores remain
111 almost undisturbed (Monroy *et al*., 2010; Mašín, 2013). Therefore, Bishop's
112 parameter χ can be considered as the effective degree of saturation of macro-pores $S_{\mathrm{r}}^{\mathrm{e}}$
113 (Alonso *et al*., 2010):

114 $$\chi = S_{\mathrm{r}}^{\mathrm{e}} = \frac{S_{\mathrm{r}} - S_{\mathrm{r}}^{\mathrm{m}}}{1 - S_{\mathrm{r}}^{\mathrm{m}}} \quad (5)$$

115 where $S_{\mathrm{r}}^{\mathrm{m}}$ the degree of saturation of micro-pores. This method can improve the
116 prediction of effective stress, but still overestimates the contribution of suction in
117 some cases (Sheng *et al*., 2011; Zhai *et al*., 2019).

118 In this study, a new method for determining χ using the macro-PSD is proposed,
119 which satisfies Houlsby's power equation.

120 **DETERMINING BISHOP'S PARAMETER χ BASED ON MACROPOROSITY**

121 Fig. 1 shows a conceptual sketch of water retention curves at two different void ratios
122 (Vaunat & Casini, 2017). The incremental change in water ratio δe_{w} (path OB) caused
123 either by suction change or mechanical loading can be split into δe_{w1} (path OA) and
124 δe_{w2} (path AB). The change of water content along path OA is caused by the increment
125 of suction at constant volume, while the incremental component of path AB is caused
126 by the change of void ratio under constant suction (net stress effect). This latter can
127 be expressed as a proportion of total volume change (Vaunat & Casini, 2017). The
128 total incremental work input per unit volume in unsaturated soils δw (Houlsby, 1997)

can be expressed as:

$$\delta w = -[\sigma - \alpha u_{\mathrm{w}} - (1-\alpha)u_{\mathrm{a}}]\frac{\delta V_V}{V} - (u_{\mathrm{a}} - u_{\mathrm{w}})\frac{\delta V_{\mathrm{w1}}}{V}$$

$$= -[\sigma - \alpha u_{\mathrm{w}} - (1-\alpha)u_{\mathrm{a}}]\delta\varepsilon_V - (u_{\mathrm{a}} - u_{\mathrm{w}})\frac{\delta V_{w1}}{V} \quad (6)$$

where σ is the total mean stress; V is the total soil volume; V_V is the volume of voids; δV_{w1} is the change of volume occupied by water due to suction; α is the ratio of the increment of volume occupied by water caused by the incremental volumetric strain under constant suction to the pore volume increment. As the first term between brackets in Eq. (6) expresses Bishop's effective stress, Vaunat & Casini (2017) proposed:

$$\chi = \alpha = \frac{\delta V_{\mathrm{w2}}}{\delta V_{\mathrm{V}}} = \frac{\delta e_{\mathrm{w2}}}{\delta e} \quad (7)$$

where δe_{w2} is the increment of water ratio caused by the change of volumetric strain under constant suction; δe is the increment of void ratio.

Fig. 2 shows the SWRCs under different void ratios for several soils (Li *et al*., 2007; Salager *et al*., 2013; Seiphoori *et al*., 2014; Gao & Sun, 2017). It appears that in low suction range, the water retention curve is dependent on void ratio. By contrast, in higher suction range, the SWRCs are almost the same (Fig. 3). The separating point corresponds to the delimitation between the range of capillary water in macro-pores and the range of adsorbed water in micro-pores (Romero, 1999). Mašín (2013) also discussed the structure evolution with mechanical loading and assumed that loading (compaction) influenced predominantly the macro-pores, while micro-pores remained untouched (Fig. 3). Thus, as the volume change is mainly due to macro-pores changes, Bishop's parameter χ is solely related to the low suction range (Fig. 3). Thereby, Eq.

(7) is modified as:

$$\chi = \frac{\delta e_{\mathrm{w2}} - \delta e_{\mathrm{w}}^{m}}{\delta e - \delta e^{\mathrm{m}}} \tag{8}$$

where $\delta e_{\mathrm{w}}^{m}$ is the incremental microscopic water ratio; δe^{m} is the incremental microscopic void ratio. In Fig. 3, two SWRCs at different void ratios should be provided and the void ratio of every SWRC should be kept constant in the whole suction range. However, in a SWRC test, the void ratio changes with suction changes. As the pore size distribution (PSD) obtained by Mercury Intrusion Porosimetry (MIP) test can be used to determine the SWRC at a constant void ratio (Zhang *et al*., 2018), the parameters in Eq. (8) can be obtained using two different PSDs, as illustrated in Fig. 4.

EVALUATION OF THE PROPOSED METHOD THROUGH SHEAR STRENGTH

Bishop & Blight (1963) described the shear strength of unsaturated soils by:

$$\tau_f = c' + [(\sigma_{\mathrm{n}} - u_{\mathrm{a}}) + \chi(u_{\mathrm{a}} - u_{\mathrm{w}})] \tan\theta' \tag{9}$$

where τ_f is the shear strength; c' is the effective cohesion at saturated state; σ_n is the normal stress; θ' is the internal friction angle. Using Eq. 9 and considering triaxial conditions, parameter χ can be back-calculated, as follows:

$$\chi = \frac{\frac{q_{\mathrm{f}} - c' \frac{6\cos\theta'}{3-\sin\theta'}}{M} - \bar{p}}{s} \tag{10}$$

where q_{f} is the deviator stress at failure; M=6 sin ϕ'/(3−sin ϕ') is the slope of critical state line; $\bar{p}$=[σ_1+2σ_3]/3-u_{a} is the net mean stress.

The results from the tests on Nanyang expansive clay were used to validate the

proposed method for Bishop's parameter χ determination (Fig. 8). Table 1 summarises the physical property indexes and triaxial shear parameters for this clay. Triaxial shear tests were conducted using an unsaturated triaxial testing apparatus supplied by GDS company. In order to obtain the molded samples only in drying process, all triaxial specimens were prepared by static compaction at initial water content of about 0.215 (suction is about 170 kPa) and initial dry density around 1.25 Mg/m^3. Table 2 gives a summary of the test conditions and stress paths. For tests No.1-3, suction was applied using axis-translation technique in triaxial cell, while for tests No.4 and No.5 the suctions (0.8 and 2.5 MPa, respectively) were applied through controlling the water contents (w=14.8% and w=12.55%, respectively) by referring to the SWRC in drying process. For higher suctions, *i.e*. tests No.6-8, the vapor equilibrium method was employed. When the samples of tests No.4-8 reached the target respective suctions, they were put into triaxial cell for further consolidation and shear tests following the stress and suction paths shown in Figs. 5 (a) and (b). The net confining pressure was 100 kPa, and the suctions were 0.05, 0.2, 0.4, 0.8, 2.5, 3.29, 38 and 368 MPa, respectively. In the triaxial shear tests, q_f and $\bar{p}$ were measured for every suction state and given in Table 3. As illustrated in Fig. 2, when the suction is higher than a specific value, the water retention curve is independent of void ratio. In addition, the modulus of soils with high suction are normally very large and the changes of void during shear tests are thus small. Thereby, shear tests under constant water content are often considered as under constant suction in high suction range (Gao *et al.*, 2019; Zhang *et al*., 2020). Substitution of q_f, $\bar{p}$, c' $\theta'$and s (see Tables 1, 2 and 3) into Eq. (10)

194 allows the calculation of Bishop's parameter χ for every suction (or degree of
195 saturation), as illustrated in Fig. 8.

196 As the void ratio of this sample with 3.29 MPa in shear test is 0.99, the PSD
197 curves of two samples compacted at different void ratios (0.81 and 0.92) at the same
198 constant suction of 3.29 MPa are considered. The results are shown in Fig. 6.
199 According to Lloret *et al*. (2003), the macro- and micro-pores are separated by the
200 point where the PSD becomes independent of loading. For bimodal structure, the
201 diameter at the valley bottom between the two pore size families can be considered as
202 the delimiting diameter between micro- and macro-pores. It appears from Fig. 6 that
203 the PSD curves are not affected by the compaction load when the pore diameter is
204 smaller than 4900 nm. Thereby, this diameter was taken as the boundary between
205 macro- and micro-pores. Eq. (8) can then be applied to determine Bishop's parameter
206 χ using the macro-PSDs. Fig. 7 shows the obtained results. For comparison, the
207 parameters in Table 1 are substituted into Eq. (10), and several other methods are
208 applied including Bishop's method with $\chi = S_r$ (Eq. 2), Vanapalli *et al*.'s method (Eq.
209 3), Zhou *et al*.'s method (Eq. 4), Alonso *et al*.'s method (Eq. 5), and Vaunat & Casini's
210 method (Eq. 7). Results are included in Fig. 8. It is observed that when the global
211 degree of saturation (Eq. 2) is considered as Bishop's parameter χ, significant
212 overestimation of suction contribution is obtained, in agreement with the observation
213 of Alonso *et al*. (2010) and Zhou *et al*. (2016). In Zhou *et al*.'s method, the capillary
214 water is separated from the adsorbed water. Then the capillary degree of saturation
215 (Eq. 4) is used to determine Bishop's parameter χ. Fig. 7 shows the fitted SWRCs by

Zhou *et al*.' SWRC method (Zhou *et al*., 2016) and the corresponding parameters. The relationship between capillary degree of saturation and degree of saturation is plotted in Fig. 8. It appears that this method underestimates the suction contribution to Bishop's effective stress over a wide suction range. In Alonso *et al*.'s method, $S_{\mathrm{r}}^{\mathrm{m}}$ is the degree of saturation of the micro-pores with diameter smaller than 4900 nm. It was found to be about 20% by calculation based on the PSD in Fig. 6. The effective degree of saturation (Eq. 5) is used to determine χ. It appears that the prediction is improved, but the suction contribution is overestimated. Similarly, Vaunat & Casini's method can improve the prediction in the low suction range as Alonso *et al*.'s method, but remains unsatisfactory in the higher suction range. In particular, a small bump on the curve obtained by Vaunat & Casini's method appears in the range of degree of saturation from 5% to 40%, owing to the contribution of micro-pores to the calculation of χ. In Vanapalli *et al*.'s method, a value of 1.6 was fitted for exponent parameter λ. It is observed that the prediction matches the test data well in the low suction range, but gives higher χ values in higher suction range. Interestingly, the proposed method (Eq. 8) shows a good agreement with the experimental results in the full suction range.

CONCLUSIONS

The hydro-mechanical behavior of unsaturated soils is strongly related to the water distribution in pores. As loading and drying predominantly affect the macro-pores, with the micro-pores remaining almost undisturbed, the pore size below which the PSD curves become independent of loading or drying processes can be considered as the delimiting diameter between macro-and micro-pores. This also implies that the

contribution of suction to Bishop's effective stress is only related to the water in macro-pores.

Based on a method proposed by Vaunat & Casini (2017) for Bishop's parameter χ determination, a modified method was proposed considering the contribution of capillary water in macro-pores. Bishop's parameter χ was defined as the ratio of the change in -water volume to the change in macro-pores during a loading process at constant suction. When the degree of saturation of macro-pores is zero, χ becomes zero too. The proposed method was evaluated using experimental shear strength data and compared with different methods reported in literature. It appeared that the proposed method allows good agreement between the prediction and measurement over a wide suction range, as opposed to other methods which either overestimate or underestimate the suction contribution to the effective stress. It is however worth noting that more test results are needed to further validate the proposed method.

ACKNOWLEDGEMENTS

The authors are grateful to the China Scholarship Council (CSC grant No. 201806060075), Ecole des Ponts ParisTech and Guilin University of Technology.

256 **References**

257 Alonso, E. E., Pereira, J. M., Vaunat, J. & Olivella, S. (2010). A microstructurally-
258 based effective stress for unsaturated soils. *Géotechnique* **60**, No. 12, 913-925.

259 Bishop, A. W. (1959). The principle of effective stress. Tek. Ukebl.**106**, No. 39, 859-
260 863.

261 Bishop, A. W. & Blight, G. E. (1963). Some aspects of effective stress in saturated
262 and partly saturated soils. *Géotechnique* **13**, No. 3, 177-197.

263 Coleman J.D.1962. Stress strain relations for partly satured soil. Correspondence,
264 Géotechnique **12**, No. 4, 348-350.

265 Cui Y. J. & Delage P. (1996). Yielding and plastic behaviour of an unsaturated
266 compacted silt. *Géotechnique* **46**, No. 2, 291-311.

267 Fredlund, D. G. & Morgenstern, N. R. (1977). Stress state variables for unsaturated
268 soils. *J. Geotech. Geoenviron. Engng* **103** (ASCE 12919).

269 Gao, Y. & Sun, D. A. (2017). Soil-water retention behavior of compacted soil with
270 different densities over a wide suction range and its prediction. *Comput. Geotech.*
271 **91**, 17-26.

272 Gao, Y., Sun, D., Zhou, A. & Li, J. (2018). Effect of stress state on soil-water retention
273 and its application on the strength prediction. *Géotech. Lett.* **8**, No. 4, 324-329.

274 Gao, Y., Sun, D. A., Zhu, Z., & Xu, Y. (2019). Hydromechanical behavior of
275 unsaturated soil with different initial densities over a wide suction range. *Acta*
276 *Geotech.*, 14(2), 417-428.

277 Gao, Y., Sun, D. A., Zhou, A., & Li, J. (2020). Predicting Shear Strength of

278 Unsaturated Soils over Wide Suction Range. Int. J. Geomech. 20, No.2, 04019175.
279 Garven, E. A. & Vanapalli, S. K. (2006). Evaluation of empirical procedures for
280 predicting the shear strength of unsaturated soils. In Unsaturated Soils 2006 (pp.
281 2570-2592).
282 Houlsby, G. T. (1997). The work input to an unsaturated granular material.
283 *Géotechnique* **47**, No. 1, 193-6.
284 Konrad, J. M. & Lebeau, M. (2015). Capillary-based effective stress formulation for
285 predicting shear strength of unsaturated soils. *Can. Geotech. J*. **52**, No. 12, 2067-
286 2076.
287 Li, J., Sun, D. A., Sheng, D. C., Sloan, S. & Fredlund, D. G. (2007). Preliminary study
288 on soil water characteristics of Maryland clay. *In Proceedings of the 3rd Asian*
289 *Conference on Unsaturated Soils*, Nanjing, China, 569-574.
290 Liu, Y., Wei, C. F., Zhao, C. G., Fang, Q. & Li, J. (2018). Work input for unsaturated
291 soils considering interfacial effects. *Int. J. Numer. Anal Methods in Geomech*. **42**,
292 No. 9, 1078-1094.
293 Lloret, A., Villar, M. V., Sanchez, M., Gens, A., Pintado, X. & Alonso, E. E. (2003).
294 Mechanical behaviour of heavily compacted bentonite under high suction changes.
295 *Géotechnique* **53**, No. 1, 27-40.
296 Lu, N., Godt, J. W. & Wu, D. T. (2010). A closed-form equation for effective stress
297 in unsaturated soil. *Water Resour. Res*. **46**, No. 5.
298 Mašín, D. (2013). Double structure hydromechanical coupling formalism and a model
299 for unsaturated expansive clays. *Engng Geol.* **165**, 73-88.

300 Monroy, R., Zdravkovic, L. & Ridley, A. (2010). Evolution of microstructure in
301 compacted London Clay during wetting and loading. *Géotechnique* **60**, No. 2, 105-
302 119.
303 Pereira, J. M., Wong, H., Dubujet, P., & Dangla, P. (2005). Adaptation of existing
304 behaviour models to unsaturated states: application to CJS model. *Int. J. Numer.*
305 *Anal. Methods Geomech.*, **29**, No. 11, 1127-1155.
306 Romero Morales, E. E. (1999). Characterisation and thermo-hydro-mechanical
307 behaviour of unsaturated Boom clay: an experimental study. Ph.D. thesis.
308 Universitat Politècnica de Catalunya.
309 Salager, S., Nuth, M., Ferrari, A. & Laloui, L. (2013). Investigation into water
310 retention behaviour of deformable soils. *Can. Geotech. J.* **50**, No. 2, 200-208.
311 Seiphoori, A., Ferrari, A. & Laloui, L. (2014). Water retention behaviour and
312 microstructural evolution of MX-80 bentonite during wetting and drying cycles.
313 *Géotechnique* **64**, No. 9, 721-734.
314 Sheng, D., Sloan, S. W. & Gens, A. (2004). A constitutive model for unsaturated soils:
315 thermomechanical and computational aspects. *Comput. Mech.* **33**, No. 6, 453-465.
316 Sheng, D., Zhou, A. & Fredlund, D. G. (2011). Shear strength criteria for unsaturated
317 soils. *Geotech. Geol. Eng*. **29**, No. 2, 145-159.
318 Vanapalli, S. K., Fredlund, D. G., Pufahl, D. E. & Clifton, A. W. (1996). Model for
319 the prediction of shear strength with respect to soil suction. *Can. Geotech. J.* **33**,
320 No. 3, 379-392.
321 Vaunat, J. & Casini, F. (2017). A procedure for the direct determination of Bishop's

322 chi parameter from changes in pore size distribution. *Géotechnique* **67**, No. 7, 631-
323 636.
324 Wheeler, S. J., Sharma, R. S. & Buisson, M. S. R. (2003). Coupling of hydraulic
325 hysteresis and stress–strain behaviour in unsaturated soils. *Géotechnique* **53**, No.
326 1, 41-54.
327 Zhai, Q. Rahardjo, H., Satyanaga, A., & Dai, G. (2019). Estimation of unsaturated
328 shear strength from soil-water characteristic curve. *Acta Geotech*. **14**, 1977-1990.
329 Zhang, F., Cui, Y., Zeng, L., Robinet, J. C., Conil, N. & Talandier, J. (2018). Effect
330 of degree of saturation on the unconfined compressive strength of natural stiff
331 clays with consideration of air entry value. *Engng Geol*. **237**, 140-148.
332 Zhang, J., Niu, G., Li, X. & Sun, D. A. (2020). Hydro-mechanical behavior of
333 expansive soils with different dry densities over a wide suction range. *Acta*
334 *Geotech.* **15**, No. 1, 265-278.
335 Zhou, A., Huang, R. & Sheng, D. (2016). Capillary water retention curve and shear
336 strength of unsaturated soils. *Can. Geotech. J*. **53**, No. 6, 974-987.
337 Zhou, A., Wu, S., Li, J. & Sheng, D. (2018). Including degree of capillary saturation
338 into constitutive modelling of unsaturated soils. *Comput Geotech*. **95**, 82-98.

Table captions.

Table 1 Physical property indexes and shear strength parameters of Nanyang weakly expansive soil

Table 2 Relevant state variables in triaxial tests

Table 3 Stress state at triaxial shear failure

Figure captions.

Fig. 1 Partition of total water volume change into components due to suction and deformation only for a path going from the water retention curve at e to $e+\delta e$ (after Vaunat & Casini, 2017)

Fig. 2. SWRCs under different void ratios over a wide suction range for soils: (a) a clayey silty sand (data from after Salager et al., 2013); (b) MX-80 granular bentonite (data from Seiphoori et al., 2014); (c) Maryland clay (data from Li et al., 2007); (d) Pearl clay (data from Gao & Sun, 2017)

Fig. 3 Sketches of soil-water retention behavior of specimens with different densities over a wide suction range

Fig. 4 PSDs at two different void ratios (compacted at different void ratios at a constant suction)

Fig. 5 Stress and suction paths for tests: (a) tests in the lower suction range; (b) tests in the higher suction range

Fig. 6 The PSD of Nanyang weakly expansive soil and the criterion adopted to discriminate macro- and micro-pores

Fig. 7 Measured SWRC and fitted curves from Zhou et al.' SWRC method (2016) for Nanyang weakly expansive soil

Fig. 8 Comparison of measured Bishop's parameter χ with the predictions obtained by various methods for Nanyang weakly expansive soil

365 **Table 1 Physical property indexes and shear strength parameters of Nanyang weakly expansive**
366 **soil**

Specific gravity	Liquid limit (%)	Plastic limit (%)	Plasticity index	Shrinkage limit (%)	Maximum dry density (g/cm^3)	Optimum water content (%)	Free swelling ratio (%)	Effective cohesion（kPa）	Effective friction angle (°)
2.74	38.8	17.2	21.6	10.5	1.69	18.2	53.8	10.4	20.8

367
368

369 **Table 2 Relevant state variables in triaxial tests**

Test No.	Molding state			Before triaxial shearing			Suction (MPa)	Control suction method	Net cell pressure (kPa)
	w_0	S_{r0}(%)	e_0	w	S_r(%)	e			
1	21.50	48.45	1.216	24.14	79.13	0.826	0.05	Axis-translation technique	100
2	22.01	50.13	1.203	19.12	52.79	0.982	0.20		
3	21.50	48.97	1.203	17.07	45.30	1.02	0.40		
4	21.64	49.54	1.197	14.80	38.44	1.04	0.80	Air-drying	
5	21.78	49.57	1.204	12.55	35.52	0.957	2.50		
6	21.86	49.95	1.199	11.90	32.53	0.996	3.29	Vapor equilibrium technique	
7	21.72	49.51	1.202	6.60	19.57	0.924	38.0		
8	21.76	49.52	1.204	4.10	12.20	0.907	367.5		

370

371 **Table 3 Stress state at triaxial shear failure**

Test No.	Control suction method	Net cell pressure (kPa)	Deviator stress q_f (kPa)	Net mean stress $\bar{p}$ (kPa)
1	Axis-translation technique	100	140	146
2			210	160
3			280	196
4	Air-drying		320	210
5			600	300
6	Vapor equilibrium technique		660	326
7			1290	550
8			1680	660

372

373

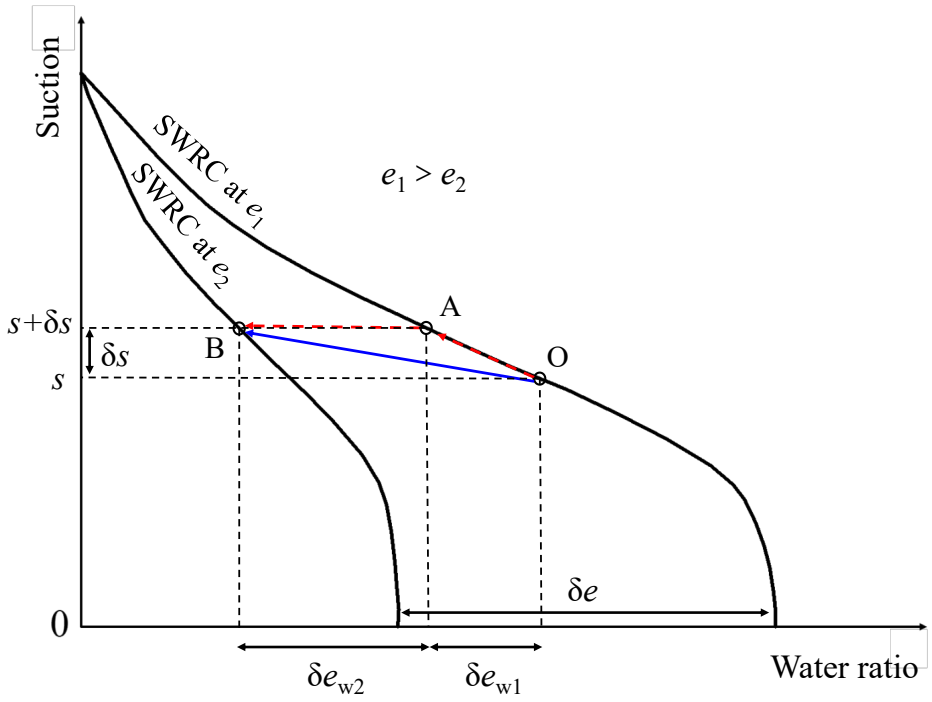

374

375 Fig. 1. Partition of total water volume change into components due to suction and
376 deformation only for a path going from the water retention curve at e to $e+\delta e$ (after
377 Vaunat & Casini, 2017)

378

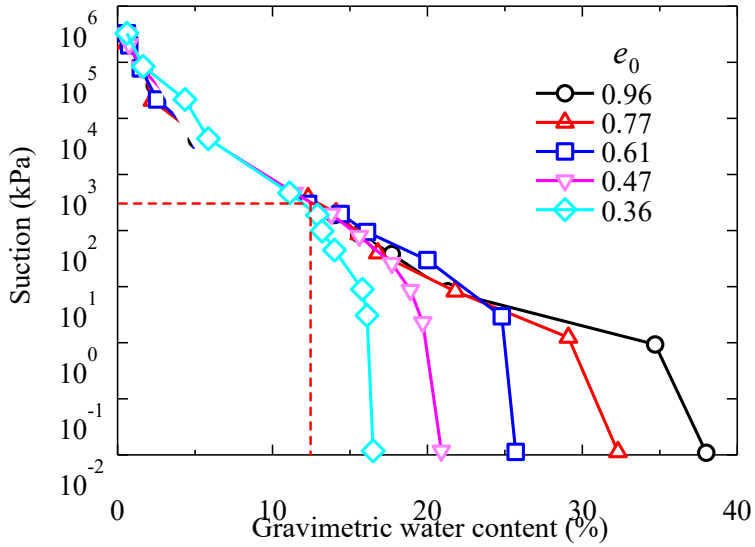
Suction (kPa)
Gravimetric water content (%)
e_0
0.96
0.77
0.61
0.47
0.36

(a)

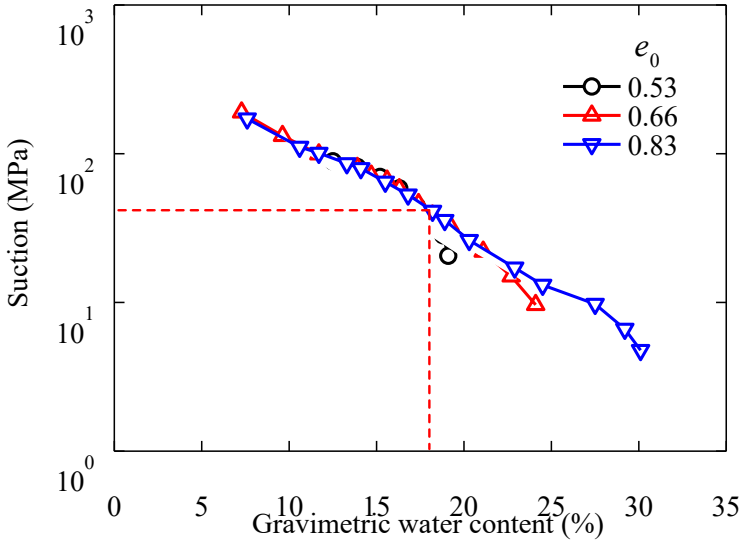
Suction (MPa)
Gravimetric water content (%)
e_0
0.53
0.66
0.83

(b)

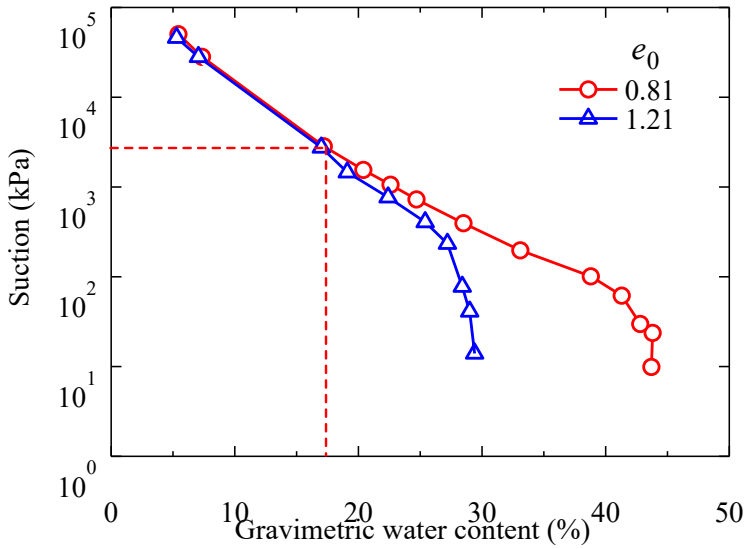

382 (c)

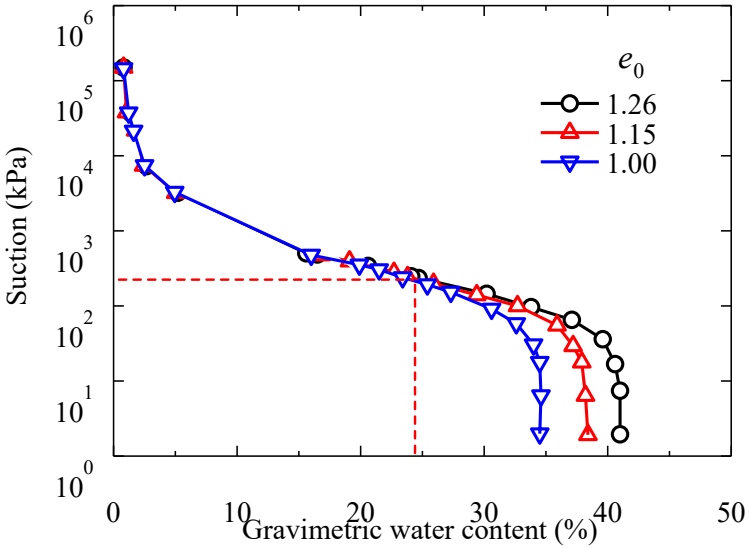

383 (d)

384 Fig. 2. SWRCs under different void ratios over a wide suction range for soils: (a) a
385 clayey silty sand (data from after Salager *et al*., 2013); (b) MX-80 granular bentonite
386 (data from Seiphoori *et al*., 2014); (c) Maryland clay (data from Li *et al*., 2007); (d)
387 Pearl clay (data fron Gao & Sun, 2017)

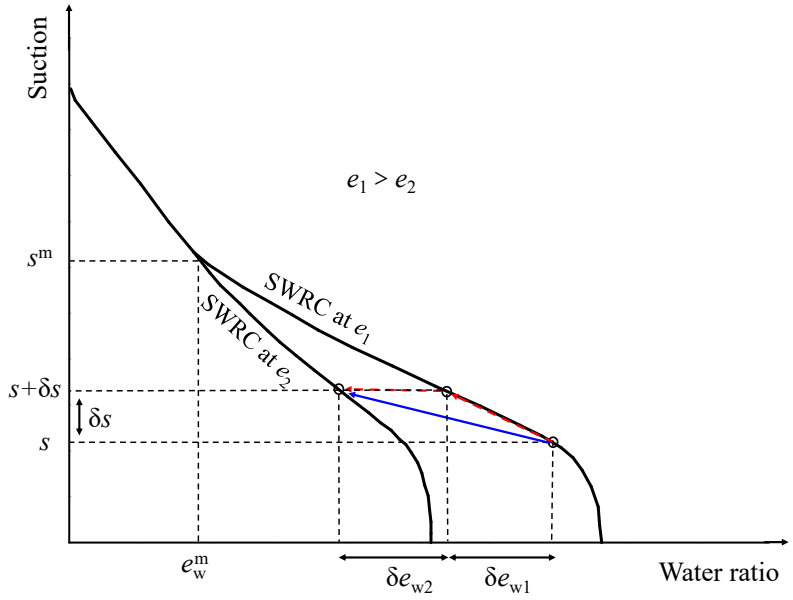

Fig. 3. Sketches of soil-water retention behavior of specimens with different densities over a wide suction range

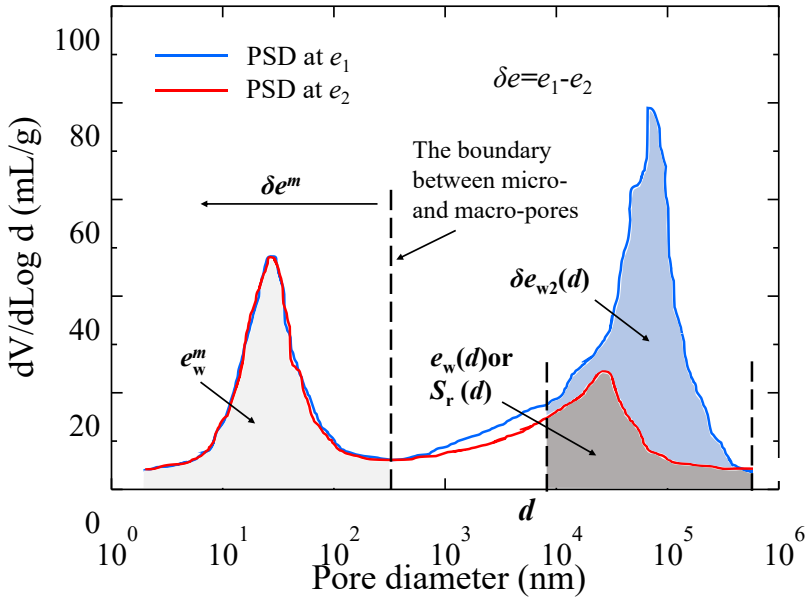

Fig. 4. PSDs at two different void ratios (compacted at different void ratios at a constant suction)

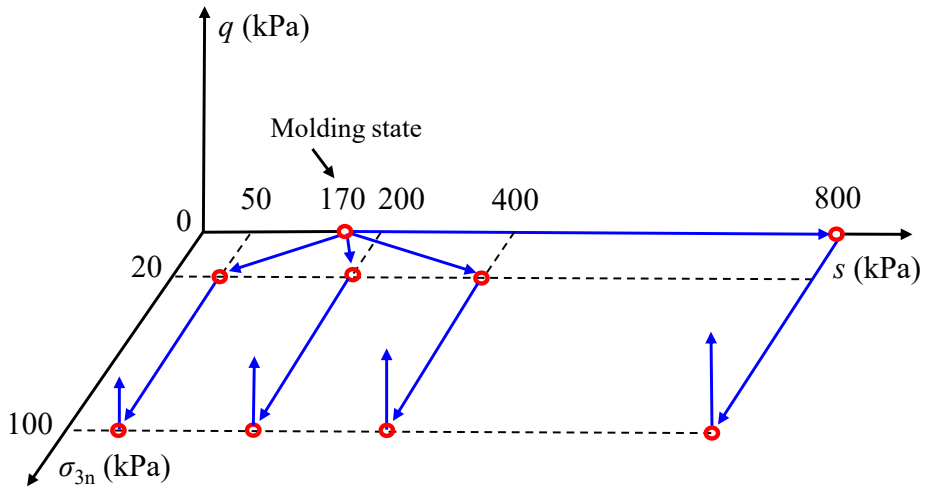

(a)

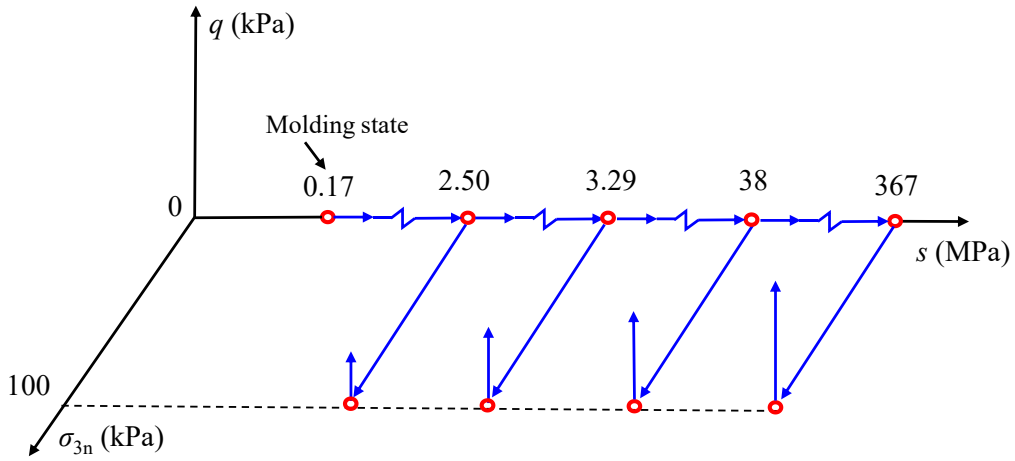

(b)

Fig. 5. Stress and suction paths for tests: (a) tests in the lower suction range; (b) tests in the higher suction range

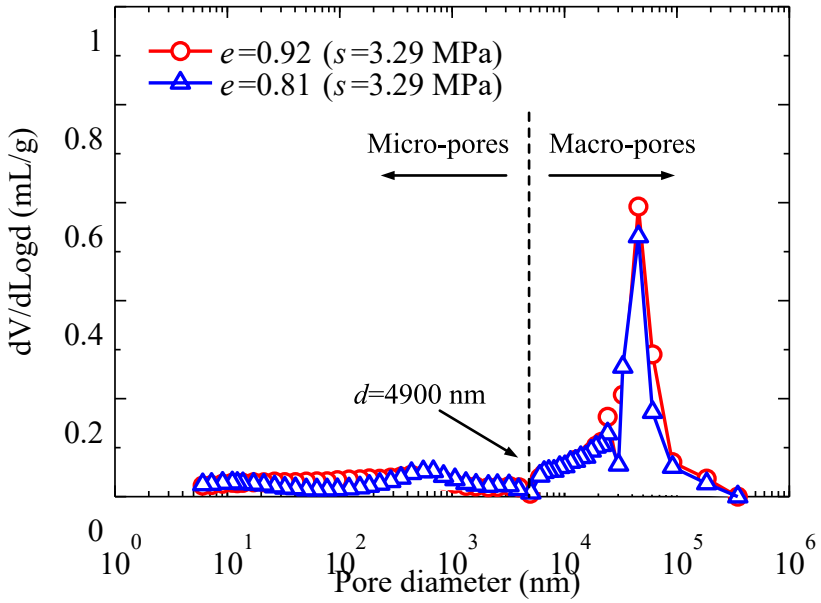

Fig. 6. The PSDs of Nanyang weakly expansive soil and the criterion adopted to discriminate macro- and micro-pores

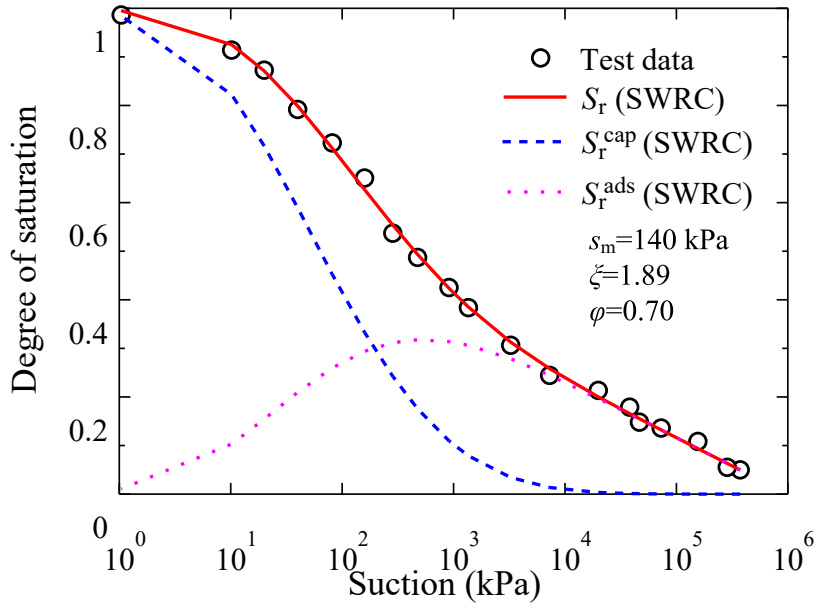

Fig. 7 Measured SWRC and fitted curves from Zhou *et al.*' SWRC method (2016) for Nanyang weakly expansive soil

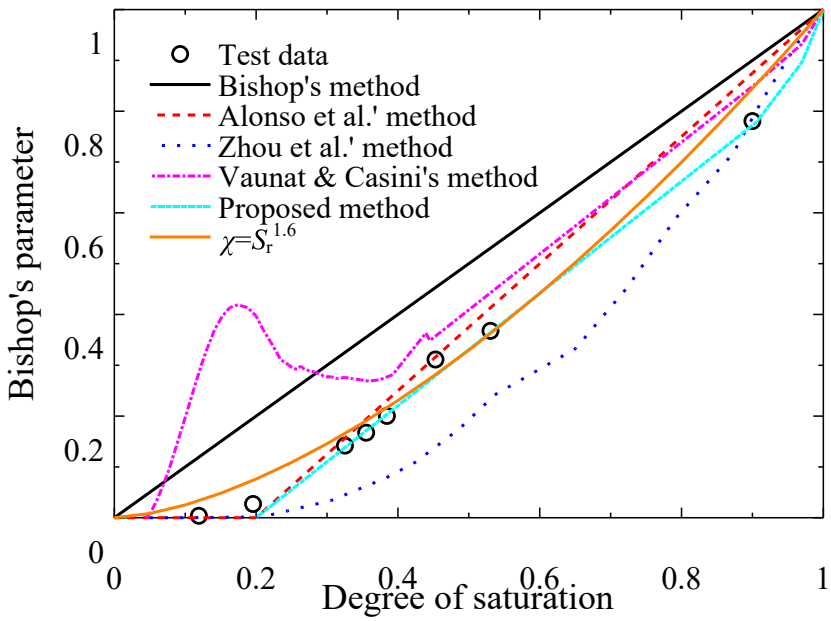

407

408 Fig. 8. Comparison of measured Bishop's parameters χ with the predictions obtained

409 by various methods for Nanyang weakly expansive soil